Received: 11 December 2019 | Revised: 3 May 2020 | Accepted: 5 June 2020

DOI: 10.1002/bit.27457

ARTICLE

BIOTECHNOLOGY BIOENGINEERING WILEY

Simulated oxygen and glucose gradients as a prerequisite for predicting industrial scale performance a priori

Maike Kuschel | Ralf Takors

Institute of Biochemical Engineering, University of Stuttgart, Stuttgart, Germany

Correspondence
Ralf Takors, Institute of Biochemical Engineering, University of Stuttgart, Allmandring 31, 70569 Stuttgart, Germany.
Email: takors@ibvt.uni-stuttgart.de

Funding information
Deutsche Forschungsgemeinschaft, Grant/Award Number: TA 241/5–2

Abstract

Transferring bioprocesses from lab to industrial scale without loss of performance is key for the successful implementation of novel production approaches. Because mixing and mass transfer is usually hampered in large scale, cells experience heterogeneities eventually causing deteriorated yields, that is, reduced titers, productivities, and sugar-to-product conversions. Accordingly, reliable and easy-to-implement tools for a priori prediction of large-scale performance based on dry and wet-lab tests are heavily needed. This study makes use of computational fluid dynamic simulations of a multiphase multi-impeller stirred tank in pilot scale. So-called *lifelines*, records of 120,000 *Corynebacterium glutamicum* cells experiencing fluctuating environmental conditions, were identified and used to properly design wet-lab scale-down (SD) devices. Physical parameters such as power input, gas hold up, $k_L a$, and mixing time showed good agreement with experimental measurements. Analyzing the late fed-batch cultivation revealed that the complex double gradient of glucose and oxygen can be translated into a wet-lab SD setup with only few compartments. Most remarkably, the comparison of different mesh sizes outlined that even the coarsest approach with a mesh density of 1.12×10^5 #/m^3 was sufficient to properly predict physical and biological readouts. Accordingly, the approach offers the potential for the thorough analysis of realistic industrial case scenarios.

KEYWORDS

cellular lifelines, CFD, double gradient, stirred tank

1 | INTRODUCTION

The transformation of current chemical industry into a sustainable, circular economy demands the successful implementation of large-scale production processes accessing the low-value, high-volume products of tomorrow. Emerging fields are the production of amino acids and organic acids (Becker & Wittmann, 2012; Morrison & Lähteenmäki, 2017). Typically, microbial hosts are the most important production platforms with *Corynebacterium glutamicum* being one of the established producers (Leuchtenberger, Huthmacher, & Drauz, 2005; Takors et al., 2007). Stirred tank reactors, still the preferred choice of large-scale production, show reduced power-per-volume ratios with increasing reactor size (Junker, 2004). Consequently, scale-up from smaller laboratory scales is usually hampered due to limited mixing and mass transfer, leading to the formation of substrate and gas gradients. The repeated exposure of cells to these fluctuating microenvironmental conditions cause unwanted reduction of productivities, conversion yields, and rising by-product formations (Bylund, Collet, Enfors, & Larsson, 1998; Enfors et al., 2001; Garcia-Ochoa & Gomez, 2009; Hewitt & Nienow, 2007;

Junne, Klingner, Itzeck, Brand, & Neubauer, 2012; Neubauer et al., 2013; Schmidt, 2005; Vrábel et al., 2001). Accordingly, tools are needed to reliably predict large-scale impacts while studying the microbial system in lab-scale. Different wet-lab scale-down (SD) devices have been developed (Käß, Junne, Neubauer, Wiechert, & Oldiges, 2014; Löffler et al., 2016). Commonly, their design is motivated by mixing time studies of large tanks that tend to overestimate the residence time of microbes in stressful zones of the bioreactor.

On the other hand, computational fluid dynamics (CFD) gain momentum to provide detailed information on environmental conditions inside a fermenter (Morchain, Gabelle, & Cockx, 2014; Pigou & Morchain, 2015) since the pioneering studies of Lapin, Schmid, and Reuss (2006). In the recent years, substrate gradients in industrial scale fed-batch production were successfully simulated outlining the impact of concentration fluctuations on microorganisms by comprehensive statistical analysis (Haringa, Deshmukh, Mudde, & Noorman, 2017; Haringa et al., 2016; Kuschel, Siebler, & Takors, 2017). Thereof, principles of SD design may be derived. Yet, the influence of oxygen as substrate in CFD simulations is often left aside. Instead, single-phase studies are performed assuming saturated dissolved oxygen levels in the entire bioreactor.

Properly considering the additional oxygen impact in stirred tank reactors (STRs) via a gaseous phase is a challenging task. Fundamental problems need to be tackled that can be grouped in (a) momentum balancing mimicked by proper drag force modeling (Bakker & Van den Akker, 1994; Brucato, Grisafi, & Montante, 1998; Buffo, Vanni, Renze, & Marchisio, 2016; Ishii & Zuber, 1979; Scargiali, D'Orazio, Grisafi, & Brucato, 2007; Tomiyama, Kataoka, Zun, & Sakaguchi, 1998), (b) bubble size distribution modeling (Hagesaether, Jakobsen, & Svendsen, 2002; Haringa et al., 2017; Kumar & Ramkrishna, 1996; Laakkonen, Moilanen, Alopaeus, & Aittamaa, 2007b), (c) modeling of bubble breakage and coalescence (Alopaeus, Koskinen, & Keskinen, 1999; Laakkonen, Alopaeus, & Aittamaa, 2006; Luo & Svendsen, 1996; Kálal, Jahoda, & Fort, 2014), and (d) mesh size impacts.

Regarding (d), all models have a strong dependency on the turbulent dissipation rate in common. The Reynolds average Navier–Stokes (RANS) k–ε model was found to underestimate the local turbulent quantities both, in single and in multiphase conditions. In contrast, large eddy simulations are known to allow best prediction quality but are too computationally demanding for large-scale multiphase applications (Buffo et al., 2016). As a trade-off, satisfactory results of total dissipated energy simulation via RANS k–ε models can be achieved (Kysela, Konfrst, Chara, Sulc, & Jasikova, 2017). However, the prediction of turbulent variables turned out to be sensitive on the discretization schemes and grid size (Coroneo, Montante, Paglianti, & Magelli, 2011). Interesting enough, velocity field or power number N_p prediction by torque was less influenced by either discretisation scheme or grid size. The observation was further exploited by Laakkonen, Moilanen, Alopaeus, and Aittamaa (2007a) who predicted turbulent dissipation rates ε to be independent on grid size but depending on experimental torque measurements. Accordingly, a novel scaling factor was introduced.

This study takes a typical late stage fed-batch scenario with *C. glutamicum* as a model case to investigate (a) the suitability of the Laakkonen approach for multiphase modeling, (b) the minimum computational efforts needed to get proper physical and biological readouts, (c) the expected microbial responses on fluctuating environmental conditions, and (d) the lessons learned for properly designing wet-lab SD devices. Model predictions are validated by experimental data measured in a 300-L stirred tank bioreactor.

2 | MATERIALS AND METHODS

Measurements were carried out in a 300-L multi-impeller stirred bioreactor, equipped with four baffles and three Rushton turbines. Details of measurements, geometry, and parameter validation are given in Supporting Information Material A. The agitation rate was set to $N = 5$/s. Air was introduced through a ring sparger with a gas feed of 0.25 vvm. Experiments were performed in water ($\rho_L = 995.7$ kg/m^3, $\eta_L = 0.0008$ Pa·s, $\sigma_L = 0.0712$ N/m) at 30°C and ambient pressure.

2.1 | Numerical simulations

2.1.1 | Simulation setup

Three different grid sizes of the full 2π domain were adopted. Details of the meshes and simulation time intervals are given in Supporting Information Material B. Numerical simulations were conducted with the commercial software ANSYS Fluent 18.1 using the realizable k–ε RANS turbulence model and the Eulerian multiphase model including mixture model for dispersed phase turbulence. The turbulent Schmidt number was set to 0.2. Bubble size ranged from 0.1 to 16 mm, divided in 23 classes according to Hagesaether et al. (2002). The scaling factor f_{sc} was introduced based on the assumption, that mixing energy (power calculated from impeller torque P_{torque} and gassed power input P_{pneum}) converts to turbulent energy and dissipates to heat in the liquid phase (P_ε). Hence local energy dissipation ε_{local} was converted according to

$$f_{sc} = \frac{P_{pneum} + P_{torque}}{P_\varepsilon}, \tag{1}$$

$$\varepsilon_{sc} = f_{sc}\,\varepsilon_{local}. \tag{2}$$

With P_{pneum} and P_ε

$$P_{pneum} = \phi_G R T \ln\left(\frac{p_0}{p}\right), \tag{3}$$

$$P_\varepsilon = \int \alpha_L \rho_L \varepsilon dV, \tag{4}$$

and with ϕ_G as molar flow, α_L as liquid volume fraction, R as universal gas constant, T as temperature, p_0 and p as standard and actual

pressure. For P_{torque}, see Supporting Information Material A. Phase interaction models were mainly based on the recommendations by Laakkonen et al. (2007a) and implemented via user-defined function (UDF). To account for the bubble drag coefficient, the correlation of Tomiyama for isolated bubbles in slightly contaminated systems (Tomiyama et al., 1998) was used. As Tomiyama drag closure $C_{D,0}$ was obtained for bubbles in quiescent fluids, effective viscosity μ_{eff} and swarm effects were included to consider drag modification under turbulent conditions (Bakker & Van den Akker, 1994; Brucato et al., 1998; Ishii & Zuber, 1979)

$$Re_{eff} = \frac{\rho_L d|u_L - u_G|}{\eta_{eff}}, \tag{5}$$

$$\eta_{eff} = \eta_L + C_5 \rho_L \varepsilon_{sc}^{\frac{1}{3}} d^{\frac{4}{3}}, \tag{6}$$

with C_5 as 0.02 proposed by Bakker and Van den Akker (1994). Additionally, swarm effects were accounted for by

$$C_D = f(\alpha_G) C_{D,0}(Re_{eff}), \tag{7}$$

$$f(\alpha_G) = \begin{cases} (1-\alpha_G)^{C_6} & \alpha_G \leq 0.8 \\ 1 & \alpha_G > 0.8 \end{cases} \tag{8}$$

with C_6 to be −1.3 as proposed by Buffo et al. (2016). Bubble break up and coalescence were implemented as described by Laakkonen et al. (2007a) replacing the original breakup function by a simple sine function. The moving reference frame model was applied to account for agitation. All walls were set to no-slip boundary conditions for the liquid and free-slip conditions for air with one exception—to account for gas accumulation behind the blades, no-slip boundary condition was applied for air in the impeller region. The top surface of the sparger was set to velocity inlet and the initial bubble diameter was calculated with 10 mm according to the correlation of Gaddis and Vogelpohl (1986). Degassing boundary condition was applied at the liquid height of the reactor, which has been increased before simulation according to the experimental gas hold up. The second-order upwind scheme was used for spatial discretization of momentum, turbulent kinetic energy, and dissipation rate. All simulations were performed in transient mode and second-order implicit formulation until a constant gas hold up was reached. Radial velocity, turbulent dissipation rate, and mixing time were compared between the three meshes. Further details on the solution procedure and mixing time determination can be found in Supporting Information Material D and E.

2.1.2 | Inclusion of biological kinetics and regime assignments

Starting from a constant gas volume fraction, glucose feed, oxygen mass transfer, and bacterial reaction were included via UDFs. A source term for glucose was defined in a small region at the fermenter top close to the shaft with a feeding rate $F = 560\,g_S/hr$, assuming a cell concentration of $c_X = 36.5\,g_{CDW}/L$. Oxygen mass transfer was included with the volumetric mass transfer coefficient $k_L a$ according to

$$\frac{dc_{O_2,L}}{dt} = k_L a(c^*_{O_2} - c_{O_2,L}) \tag{9}$$

with $c^*_{O_2}$ as oxygen saturation concentration calculated by Henry's law and $c_{O_2,L}$ as liquid oxygen concentration. A multisubstrate kinetic suggested by Roels (1983) was used to account for substrate consumption:

$$\mu = \mu_{max} \min\left(\frac{c_S}{c_S + K_S}; \frac{c_{O2}}{c_{O_2} + K_{O_2}}\right) \tag{10}$$

with μ as growth rate and K_S and K_{O_2} as half saturation concentration. Specific growth parameters of *C. glutamicum* ATCC13032 were obtained from previous batch experiments (not published) resulting in a maximal growth rate of $\mu_{max} = 0.441\,hr^{-1}$, a biomass glucose yield of $Y_{XS} = 0.474\,g_{CDW}/g_S$ and a biomass oxygen yield of $Y_{XO_2} = 0.043\,g_{CDW}/mmol_{O_2}$. The K_S value for *C. glutamicum* $K_S = 3.6 \times 10^{-3} g_S/L$ was taken from literature (Lindner, Seibold, Henrich, Krämer, & Wendisch, 2011). The value for K_{O_2} was taken from *Escherichia coli* $K_{O2} = 2 \times 10^{-3}\,mmol_{O_2}/L$ because similar cytochrome *bd* activity has been reported (Kita, Konishi, & Anraku, 1984; Kusumoto, Sakiyama, Sakamoto, Noguchi, & Sone, 2000). Simulation ran in transient mode until steady-state concentrations of glucose and oxygen were reached. They mirror a so-called "pseudo steady-state" characterized by short-term stable gradients in turbulent flow fields. This concentration profile reflects a "snap-shot" of a late pilot-scale fed-batch scenario. Coupling the reaction to the continuous liquid phase was assumed, since mixing and mass transfer are an order of magnitude higher than the reaction. However, the flow field shows periodically changing behavior. To facilitate comparability between the three meshes, power input by torque as well as velocity profiles and turbulent dissipation rate were tracked at several positions and the simulation was stopped when average values of the examined parameters were reached. Then, the glucose and oxygen gradients were classified in specific regimes according to the growth rate substrate dependency of a single substrate Monod kinetic for either glucose or oxygen, respectively. If the dimensionless substrate concentration c_M/K_M was smaller or equal to 0.5 (corresponding to $c_M/(c_M + K_M) \leq 0.33$) a linear correlation between μ and c_M exists, referring to a low concentration regime (L_S for low glucose or L_{O_2} for low oxygen). If $c_M/K_M > 9$, the growth rate μ reaches 90% of μ_{max} and the function can be approximated by a function of zero order making μ independent of a change in substrate concentration (H_S and H_{O2}). The range in between refers to a transient regime (T_S and T_{O2}).

2.1.3 | Particle tracking

The analysis of heterogeneities via cellular lifelines within a bioreactor was previously published in various papers (Haringa

et al., 2017, 2016; Kuschel et al., 2017). The total amount of 120,000 bacteria was introduced as massless Lagrange particles (St << 1) and tracked for 260 s for each mesh. Euler and Lagrange average growth rates were compared to proof for statistical relevance. The discrete random walk model was enabled. The gradient and flow field were fixed during particle tracking. The position and the encountered glucose and oxygen concentrations for each bacterium were recorded every 15 ms. Further analysis was performed in MATLAB®.

2.1.4 | Statistical evaluation of bacterial lifelines

The further processing of the trajectories included a smoothening step by applying a moving average filter to remove unrealistic turbulent fluctuations. The filter window was based on the Lagrangian time scale as recommended by Haringa et al. (2017). Here, a second filter step to filter out rapid consecutive low-amplitude crossings is suggested which was enabled by a median filter. Then, the filtered trajectories were analyzed according to their regime transitions including frequency and duration of residences.

3 | RESULTS AND DISCUSSION

3.1 | Validation of physical parameters for different grid sizes

Multiphase simulations were performed using three different grid sizes (Supporting Information Material B). Sufficient mesh granularity is a critical aspect in CFD simulations especially for the proper estimation of the gas–liquid mass transfer. Typically, sensitive flow variables such as radial velocity and turbulent dissipation rate are checked for mesh independency. While u_{rad} already showed decent results for Mesh 1, differences between the meshes are significant for ε (Supporting Information Material D). Accordingly, the scaling factor for ε was introduced into breakup, coalescence, drag and mass transfer functions as described in Section 2.1.1. A similar scaling factor has been reported to show good results in multiphase simulations (Laakkonen et al., 2007a). Noteworthy, the scaling factor was determined from simulation in our approach. Experimental data were only required for validation purposes.

Figure 2a shows the flow field, Figure 2b shows the gas volume distribution, and Figure 2c shows the bubble size distribution of the simulation with Mesh 3. Clearly, no distinct separation of flow fields from radial pumping Rushton turbines is visible, but an overlap of vortices. The merged flow field is the result of the upward moving gas phase in combination with rather proximate impeller setting. The first impeller shows a loading regime (see Figure 2b). With the Froude number $N^2D/g = 0.52$ and the Flow number $Q_g/ND^3 = 0.02$, no flooding is expected according to critical flow numbers of Rosseburg, Fitschen, Wutz, Wucherpfennig, and Schlüter (2018) and others (Wiedmann, 1983). Own studies outlined the need to consider the impact of effective viscosity on the estimation of drag force. Otherwise, bubbles left the impeller discharge streams too early leading to nonrealistic bubble accumulation close to the blades. The lower impeller disrupted entering bubbles to 4–5 mm (see Figure 2c). Smallest bubbles of 2–3 mm were found in discharge streams of the middle and the upper Rushton turbine gaining size when they moved upwards to the liquid surface. Largest bubbles were observed at the impeller shaft close to the reactor top where coalescing effects are most dominant. This tendency is in good agreement with the experimental results by Laakkonen et al. (2007a).

Table 1 summarizes all experimental and simulated data of this study. The power input by torque is predicted well by the simulation. Especially, Mesh 3 shows less than 2.8% deviation from experimental measurements. The power number $N_P = P/\rho N^3 D^5$ of 10.88 for the entire systems is rather low compared to expected N_P of 5 per Rushton turbine in distinct turbulent flows (here $Re \approx 2.5 \times 10^5$) (Rushton, Costich, & Everett, 1950). However, such high N_P are only obtained for multi-impeller systems with complete parallel flow. By contrast, Figure 2 clearly depicts the nondistinct character of the flow field in agreement with Chunmei, Jian, Xinhong, and Zhengming (2008) and Xueming, Xiaoling, and Yulin (2008) which is further supported by the low velocity ratio of the middle stirrer (Supporting Information Material D). Taking an additional reduction of power number due to the gas phase into account, Armenante and Chang (1998) found similar non-gassed power numbers for a comparable reactor configuration. Experimental (3.6%) and simulated (3.2%) gas hold up are in fair comparison, considering the experimental noise. The simulated gas hold up of 2.4% from Laakkonen et al. (2007a) is smaller than the gas hold up presented here. Although the authors chose a higher agitation rate, one instead of three Rushton turbines was used. Therefore, smaller power input and gas hold up can be expected. Highly accurate prediction of k_La values was achieved. Even the coarse Mesh 1 still reached good prediction quality of 92.8%. We qualify the very good prediction quality of k_La as a mirror of the well suitability of the Laakkonen approach. Because f_{SC} scales the turbulent energy dissipation proportionally, small differences in the prediction precision between the meshes may exist due to the nonlinear character of k_La, breakage and drag function. Gas hold up is furthermore directly dependent on the velocity profile which is predicted slightly different by Mesh 3 (Supporting Information Material D).

Following the approach of Vasconcelos, Alves, and Barata (1995) and choosing the geometric similarity as 100, the mixing time is estimated as $\tau_{95} = 15.9$ s fairly agreeing with the experimental findings. Alternately, the mixing time was simulated by adjusting the Schmidt number Sc_T from 0.7 to 0.2. Whereas this is a common choice for single-phase studies (Delafosse et al., 2014; Haringa et al., 2016; Montante, Moštěk, Jahoda, & Magelli, 2005), the improvement is less incisive for multiphase simulations where the upwards motion of the gas breaks the mass-exchange barrier of the inter impeller zone (Haringa et al., 2017). Considering the experimental standard deviation of mixing experiments all meshes allow satisfactory prediction quality.

Because the bubble diameter was not experimentally measured, comparison is performed with measured Sauter mean diameters of about 1.2–4.1 mm from Laakkonen et al. (2007a) testing similar settings. Accordingly, fair agreement is observed.

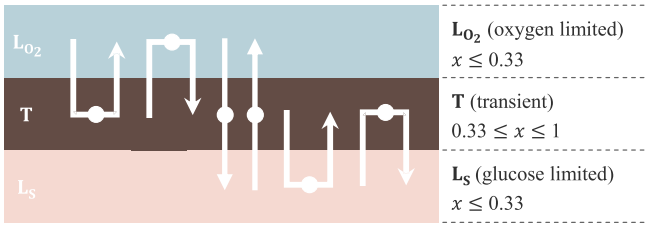

FIGURE 1 Regime transition patterns. $L_{O_2}TL_{O_2}$: Particle starts and ends in low oxygen regime with a dwelling time in the transition area. $TL_{O_2}T$: Reverse event starting in the transition area with residence in low oxygen regime. $L_{O_2}TL_S$: Particle traverses all regimes from low oxygen to low glucose. $L_STL_{O_2}$: Reverse movement from low glucose to low oxygen. TL_ST: Circulation from transition over low glucose back to transition area. L_STL_S: Reverse event from low glucose to transition back to low glucose regime. The second capital letter always indicates the area in which the residence time τ was measured [Color figure can be viewed at wileyonlinelibrary.com]

Summarizing, simulated values fit the experimental data very well. Even for Mesh 1, deviations are acceptable.

3.2 | Pseudo-stationary double gradients

Pseudo-stationary double gradients of the late fed-batch scenario were obtained by embedding reactions into the continuous phase containing the media. Estimating the time needed to shift a culture to substrate depletion ($\tau_{dep} = K_S/(q_{S,max}c_X) = 0.38$ s) reveals that τ_{dep} is more than an order of magnitude smaller than mixing ($\tau_{95} = 15.2 \pm 4$ s) and circulation time ($\tau_{circ} = 2.9 \pm 0.75$ s). Accordingly, the formation of substrate gradients is likely to occur. Figure 3 shows that spatial distributions of growth are fairly similar for each simulation (average $\mu = 0.0335$ hr^{-1}) irrespective of the mesh quality used. Highest growth rates were reached proximate to the top impeller whereas cell growth was strongly limited in the rest of the reactor. Figure 4a,b elucidates the reasons for the growth distribution highlighting glucose and oxygen gradients exemplarily of Mesh 3.

TABLE 1 Comparison of simulated parameters and experimental validation

Setup	N_P	α_G (%)	k_La (hr^{-1})	τ_{95} (s^{-1})	d_b (mm)
Mesh 1	9.50	2.7	116	17	3
Mesh 2	11.82	2.6	115	13.9	3
Mesh 3	11.18	3.2	122	13.1	3.4
Exp	10.88 ± 0.11	3.6 ± 0.3	125 ± 4	15.2 ± 4	1.2–4.1

Note: Experimental bubble diameter was taken from Laakkonen et al. (2007a).

Small differences between the meshes in the overall physical parameters like k_La or τ_{95} contributed to slight differences in the gradient formation. High glucose (H_S) concentrations only occur next to the feed port, surrounded by a transition zone (T_S), whereas the flow fields of the three Rushton turbines is glucose-limited (L_S). Interestingly, the opposite scenario attunes for oxygen showing high oxygen concentrations (H_{O_2}) in the bulk ranging from the reactor bottom to the top impeller (see Figure 4b). The overlay of glucose and oxygen gradients leads to a scenario as shown in Figure 4c, the assignment of low oxygen levels at the top (L_{O_2}), low glucose levels in the Rushton mixing zone (L_S) and a lean section of mid-level concentrations (T) located between L_{O_2} and L_S. It is exactly in T where highest growth rates occur. Interesting enough, T only accounts for <5% of the of the total volume according to Mesh 3. Notably, Meshes 1 and 2 provide similar prediction with 3.7% and 3.3%, respectively.

3.2.1 | Statistical lifeline analysis

Applying the approach of Haringa et al. (2016) so-called *lifelines* were studied, that is, the fluctuating paths of 120,000 *C. glutamicum* massless cells were recorded and analyzed with respect to the regime changes according to Figure 1. Concentration profiles of glucose and oxygen encountered by individual cells were used to

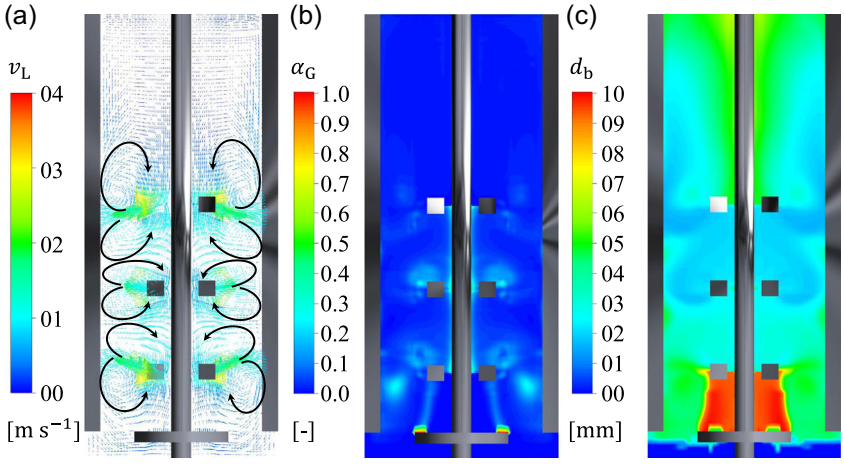

FIGURE 2 (a) Flow field, (b) gas volume distribution, and (c) bubble size distribution of the simulation with Mesh 3 [Color figure can be viewed at wileyonlinelibrary.com]

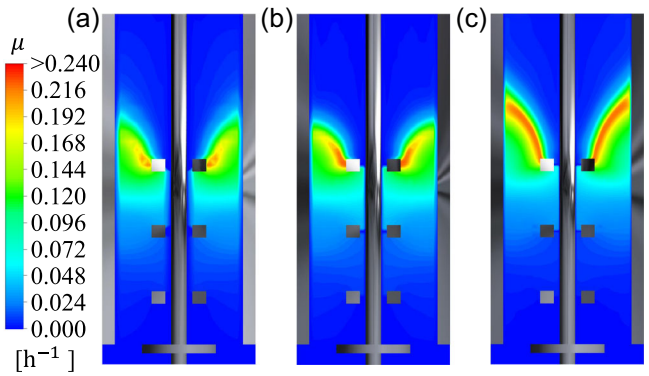

FIGURE 3 Local distribution of simulated growth rates for (a) Mesh 1, (b) Mesh 2, and (c) Mesh 3 [Color figure can be viewed at wileyonlinelibrary.com]

estimate growth rates applying the Roels multisubstrate kinetic. The average growth rate ($\mu = 0.0291\,hr^{-1}$) was comparable for all meshes and is in good agreement with the Eulerian approach ($\mu = 0.0335\,hr^{-1}$). Thereof, the conclusion was drawn that a sufficient number of particles was used. Figure 5d shows an exemplary lifeline for 25 s. The normalized glucose and oxygen concentrations are displayed in Figure 5a for 200 s. The profiles are consistent with the gradient depicted in the previous section. High glucose concentrations are coupled to low oxygen concentrations and vice versa. Only if both substrates are present in moderate concentrations higher growth rates can be obtained as demonstrated in Figure 5b. The profiles were translated into regime transitions for further analysis as illustrated in Figure 5c. Characteristic patterns are marked in red. TL_ST may serve as an example for interpretation: After 18 s, the bacterial fluctuating path TL_ST starts from moderate glucose and oxygen levels (T), traverses quickly to low glucose

FIGURE 4 Concentration profiles derived from Mesh 3 of glucose (a) fed from the top and oxygen (b) introduced by a ring sparger close to the reactor bottom. Coloration from dark to light colors indicates high, transient, or low concentrations. Overlapping both gradients results in the regimes (c) with low glucose L_S, transient T, and low oxygen L_{O_2} concentrations [Color figure can be viewed at wileyonlinelibrary.com]

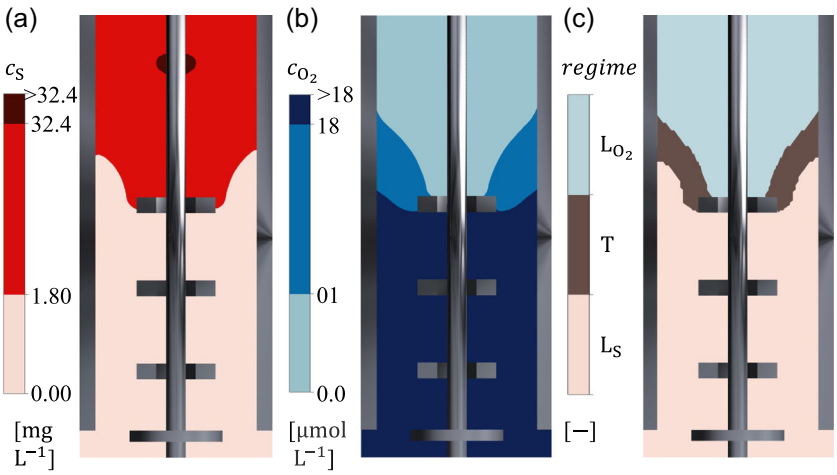

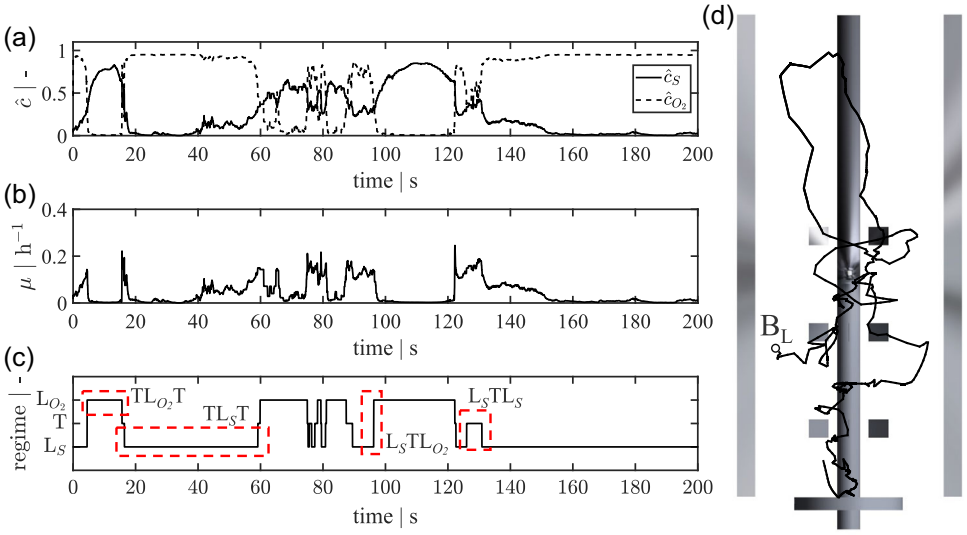

FIGURE 5 (a) Profiles of normalized ($\hat{c} = c_M/c_M K_M$) glucose and oxygen concentration and (b) the resulting growth rate of a bacterial lifeline recorded for 200 s. (c) The profiles were translated to low glucose L_S, low oxygen L_{O_2}, and a transient regime T. (d) Bacterial lifeline in the bioreactor for 25 s [Color figure can be viewed at wileyonlinelibrary.com]

TABLE 2 Regime transition statistics

Regime transition	Frequency (%)	$\bar{\tau}$ (s)	τ_{max} (s)
L_STL_S	10.06	0.36	1.05
TL_ST	31.36	5.50	75.66
$TL_{O_2}T$	26.47	2.99	13.47
$L_{O_2}TL_{O_2}$	4.62	0.38	1.23
$L_STL_{O_2}$	15.99	0.20	0.81
$L_{O_2}TL_S$	11.50	0.33	1.20

Note: Total frequency, average ($\bar{\tau}$), and maximal (τ_{max}) residence time are listed for each regime transition pattern.

concentrations (L_S) where the cells stays for 40 s before cycling back to moderate glucose and oxygen levels encoded as T. Notably, time τ code for residence periods of the middle zone (mid-capital letter) because transition times are quite short.

Bacterial lifeline patterns were statistically evaluated to obtain frequency distributions as a function of τ. Finally, six transition strategies were evaluated and compared for the three meshes. Statistical readouts comprised the total frequency of the events, average and maximal residence times (see Table 2). Maximal residence times correspond to the limit, within which 99% of the values were located. For example, Figure 6 depicts the regime transition distributions of Mesh 3. Remarkably long residence times are assessed for the regime transition TL_ST. Some bacteria may linger up to 76 s in the glucose-limited zone before moving back to the transition area. However, the average residence time in L_S is about 5.5 s. With ~31% TL_ST is the most frequent regime transition. The following reason may be deduced from Figure 3: cells are trapped in the trailing vortices of the three impellers causing circulation within the low glucose regime. The second most frequent regime transition is $TL_{O2}T$ with 26.5%. Maximum (13.5 s) and average (3 s) residence times are clearly shorter than in regime TL_ST. Notably, all distribution patterns comprising T as key residence zone show rapid decays after <1.5 s. Those regimes host cells less than 0.4 s in T which is in the magnitude of τ_{dep}. In essence, the fast crossings of zone T reflect its small dimension and the high fluid velocities at the top impeller.

Using Mesh 3 as reference, Figure 7 depicts deviations of average regime residence times regarding Meshes 1 and 2. For instance, results of L_STL_S and $L_STL_{O_2}$ differ only about 1% and 7% for Meshes 2 and 1, respectively. Most important, the dominating transitions TL_ST and $TL_{O_2}T$ only differ by max 31% (Mesh 2), with Mesh 1 showing fairly good agreement of −9.6% and +16% only. This finding is highly remarkable as it means that biologically meaningful readouts (i.e., exposure to limiting regimes) can be predicted well with moderate computational efforts. Mesh 1 only possesses 1/10 grid size of Mesh 3. In other words, less computation is needed to qualify cellular performance in large-scale industrial bioreactors.

3.2.2 | Simplified design of scale-down devices

For the given model case scenario, the volumetric fraction of moderate substrate supply (T) is less than 5% only. Transitions through this zone take 1.2 s maximum. Hence, instantaneous metabolic responses may occur, but the initiation of transcriptional effects appears rather unlikely. For *E. coli*, Löffler et al. (2016) observed massive transcriptional responses after stress exposure periods >35 s. Still, the initiation of transcriptional response may have happened causing the propagation of the transcriptional response into well-mixed zones of the bioreactor (Nieß, Löffler, Simen, & Takors, 2017). However, *C. glutamicum* has already proven its strong robustness regarding the exposure to large-scale stress conditions. Accordingly, the transition zone may be excluded for SD design leading to a simplified two-compartment SD device similar to Käß et al. (2014). As such, the Euler–Lagrangian analysis may be simplified by lumping related regime changes finally yielding the two-compartment readouts $L_SL_{O_2}L_S$ and $L_{O_2}L_SL_{O_2}$. With 3.4 s for the first and 5.7 s for the latter, longer residence times in glucose-limited regimes were found that may expand to maximum residence times of 15 and 80.5 s, respectively.

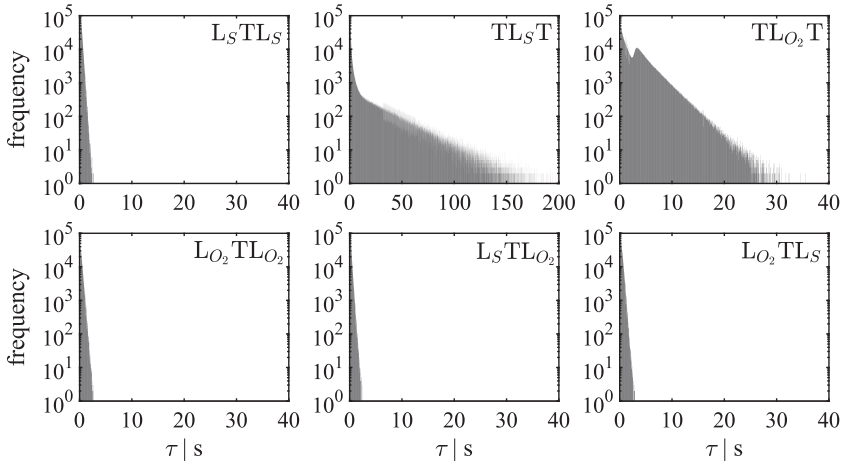

FIGURE 6 Regime transition pattern as function of the residence time τ. The six possible patterns are shown as semi-log plot

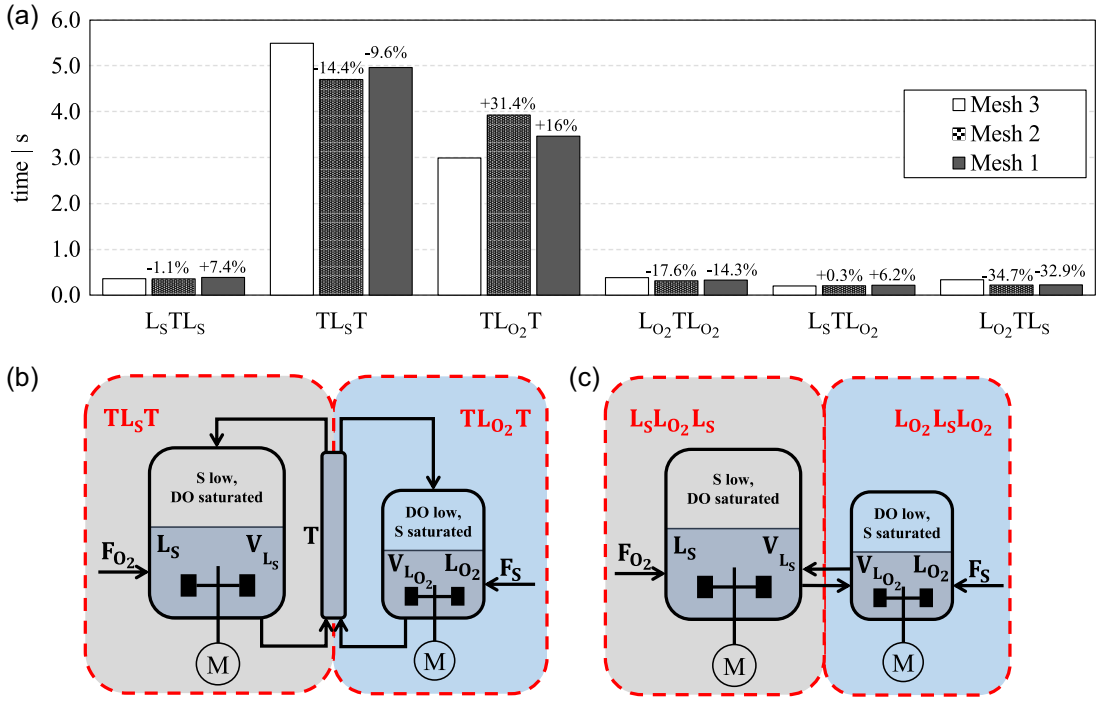

FIGURE 7 (a) Comparison of average residence time prediction $\bar{\tau}$ for the three simulated meshes. Deviations of Meshes 1 and 2 compared to Mesh 3 are displayed. (b and c) Examples of simplified scale-down devices [Color figure can be viewed at wileyonlinelibrary.com]

In general, the findings of residence time distributions may be well used to design wet-lab scale-up simulators. Figure 7b illustrates that the regimes are translated in a multicompartment setup comprising two STRs connected by a plug flow reactor (PFR). The PFR may serve as the realization of the T zone. Key limitations are installed in the STR as indicated. Each STR requires additional supply of substrate or oxygen to raise limiting levels. Pumping between PFR and both STRs follows the mindset of $L_STL_{O_2}$, L_STL_S, $L_{O_2}TL_S$, and $L_{O_2}TL_{O_2}$ traveling paths. Regime assignments and changes may be controlled by the volume ratios of the different tanks with average dwelling times set by pumping rates. By deciding on a particular scale-up design, experimentalists basically choose the percentage of frequency changes covered by the experimental setup. For instance, the showcase of Figure 7c neglects the impact of T for the sake of simplicity. Noteworthy, the examples of Figure 7b,c mirror the 300-L pilot-scale scenario. Mimicking large-scale industrial bioreactors likely requires longer dwelling times and different volume ratios.

3.2.3 | Sensitivity of regime size depending on biological parameters

Given that kinetic parameters and process conditions differ from organism to organism their impact on regime size and transitions may be an important criterion for qualifying the suitability of scale-up simulators (such as Figure 7b,c) for studying the impact of liquid nutrients and oxygen. Results of a sensitivity analysis varying kinetic and operational parameters are summed in Table 3 and depicted in Supporting Information Material F exemplarily for one scenario. Doubling the biomass concentrations c_X leads to smaller transient regime T, but to bigger regimes of limited oxygen L_{O_2} and glucose concentrations L_S. For organisms possessing higher specific maximal substrate consumption rate, the size of L_S increased, due to reduced transient regime, whereas L_{O_2} remains. The opposite scenario occurs for organisms with higher specific maximal oxygen consumption rate q_{O_2}, leaving L_S unaffected but leading to decreased T and increased L_{O_2}. Rising K_S adapts regime classification leading to bigger substrate limitation zone, smaller transient and oxygen limited zones. Higher K_{O_2} shows no effects on regime size. By doubling the feed the transient regime spreads toward the second impeller, reducing L_S but leaving L_{O_2} unaffected. Reverse behavior of the regime size was observed by lowering the respective parameter.

TABLE 3 Sensitivity of regime size

	Influence on regime size		
Parameter	L_S	T	L_{O_2}
c_X ↑	↑	↓	↑
$q_{S,max}$ ↑	↑	↓	→
$q_{O_2,max}$ ↑	→	↓	↑
K_S ↑	↑	↓	↓
K_{O_2} ↑	→	→	→
F ↑	↓	↑	→

Note: Variation of organism-specific parameter or operating conditions.

Summarizing, sensitivity analysis shows that ratios of L_S:T:L_{O_2} depend on biological kinetics and process conditions while structural settings of two-phase scale-up simulators remain. Indeed, the setup well resembles conventional settings. However, the two-phase CFD simulations give a quantitative estimate about the degree of similarity with the eyes of the microbes, now.

4 | CONCLUSION

The scaling factor approach (Laakkonen et al., 2007a, 2007b) was successfully applied for a two-phase flow Euler–Euler multi-impeller pilot-scale bioreactor simulation. Although, the factor was simply simulated and not derived from experimental measurements, physical properties such as power input, gas hold up, k_La value and mixing time were estimated fairly good compared to experimental tests. Interesting enough, statistical analysis of lifelines further revealed that biologically relevant readouts such as regime changes can be based well on relatively coarse mesh granularity, still giving accurate residence time distribution of <15% deviation (mostly) compared to 10-fold finer structured meshes. Consequently, a mesh density of 1.12×10^5 #/m^3 is suggested to be sufficient to reflect the actual situation within the bioreactor. Likewise, similar grid sizes have been used in multiphase simulations (Bach et al., 2017; Haringa et al., 2017). This finding opens the door for large-scale applications with least computational effort. Using the scaling factor not only proper estimations of physical criteria but also biological readouts such as regime changes are well predictable.

The study showcased the application for *C. glutamicum*. But sensitivity analysis showed that design and structure of wet-lab scale-up simulators should be well transferrable to other microbial kinetics and process conditions. Notably, the approach intrinsically offers an a priori quantitative assessment predicting how close lab scale conditions will mimic large-scale scenarios.

ACKNOWLEDGMENTS

The authors gratefully acknowledge the funding by Deutsche Forschungsgemeinschaft DFG (Grant No. DFG241/5-1). The authors also thank Salaheddine Laghrami for his support with the experimental measurements. Computational resources have been provided by the High Performance Computing Center Stuttgart of the University of Stuttgart.

CONFLICT OF INTERESTS

The authors declare that there are no conflict of interests.

NOMENCLATURE

C_D	drag coefficient
CO_2	oxygen concentration ($mmolo_2$/L)
c_S	glucose concentration (g_S/L)
c_X	biomass concentration (g_{CDW}/L)
F	feeding rate (g_s/hr)
f_{sc}	scaling factor
k_La	volumetric mass transfer rate (hr^{-1})
KO_2	affinity constant for oxygen ($mmolo_2$/L)
K_S	affinity constant for glucose (g_S/L)
N	agitation rate (s^{-1})
N_p	power number
P	power (W)
p	pressure (Pa)
R	universal gas constant ($J{\cdot}mol^{-1}{\cdot}K^{-1}$)
Re	Reynolds number
Sc_T	turbulent Schmidt number
St	Stokes number
T	temperature (K)
Y_{XO_2}	biomass oxygen yield (g_{CDW}/$mmol_{O_2}$)
Y_{XS}	biomass substrate yield (g_{CDW}/g_S)

ABBREVIATIONS

BSD	bubble size distribution
LES	large eddy simulation
PBE	population balance model
RANS	Reynolds average Navier–Stokes
SD	scale down
UDF	user defined function

GREEK SYMBOLS

α	volume fraction
ε	turbulent dissipation rate (m^2/s^3)
η_L	media viscosity (Pa·s)
μ	growth rate (hr^{-1})
ρ_L	media density (kg/m^3)
σ_L	media surface tension (N/m)
τ_{95}	mixing time (s)
ϕ_G	molar flow (mol/s)

SUBSCRIPTS

*	equilibrium concentration
dep	depletion
eff	effective
G	gas
L	liquid
max	maximal
sc	scaled variable

ORCID

Ralf Takors http://orcid.org/0000-0001-5837-6906

REFERENCES

Alopaeus, V., Koskinen, J., & Keskinen, K. I. (1999). Simulation of the population balances for liquid-liquid systems in a nonideal stirred tank. Part 1 Description and qualitative validation of the model. *Chemical Engineering Science*, *54*(24), 5887–5899.

Armenante, P. M., & Chang, G. M. (1998). Power consumption in agitated vessels provided with multiple-disk turbines. *Industrial and Engineering Chemistry Research*, *37*(1), 284–291.

Bach, C., Yang, J., Larsson, H., Stocks, S. M., Gernaey, K. V., Albaek, M. O., & Krühne, U. (2017). Evaluation of mixing and mass transfer in a stirred pilot scale bioreactor utilizing CFD. *Chemical Engineering Science*, *171*, 19–26.

Bakker, A., & Van den Akker, H. E. A. (1994). A computational model for the gas-liquid flow in stirred reactors. *Chemical Engineering Research and Design*, *72*(A4), 594–606.

Becker, J., & Wittmann, C. (2012). Bio-based production of chemicals, materials and fuels – *Corynebacterium glutamicum* as versatile cell factory. *Current Opinion in Biotechnology*, *23*(4), 631–640.

Brucato, A., Grisafi, F., & Montante, G. (1998). Particle drag coefficients in turbulent fluids. *Chemical Engineering Science*, *53*(18), 3295–3314.

Buffo, A., Vanni, M., Renze, P., & Marchisio, D. L. (2016). Empirical drag closure for polydisperse gas–liquid systems in bubbly flow regime: Bubble swarm and micro-scale turbulence. *Chemical Engineering Research and Design*, *113*, 284–303.

Bylund, F., Collet, E., Enfors, S., & Larsson, G. (1998). Substrate gradient formation in the large-scale bioreactor lowers cell yield and increases by-product formation. *Bioprocess Engineering*, *18*, 171–180.

Chunmei, P., Jian, M., Xinhong, L., & Zhengming, G. A. O. (2008). Investigation of fluid flow in a dual Rushton impeller stirred tank using particle image velocimetry. *Chinese Journal of Chemical Engineering*, *16*(5), 693–699.

Coroneo, M., Montante, G., Paglianti, A., & Magelli, F. (2011). CFD prediction of fluid flow and mixing in stirred tanks: Numerical issues about the RANS simulations. *Computers and Chemical Engineering*, *35*(10), 1959–1968.

Delafosse, A., Collignon, M. L., Calvo, S., Delvigne, F., Crine, M., Thonart, P., & Toye, D. (2014). CFD-based compartment model for description of mixing in bioreactors. *Chemical Engineering Science*, *106*, 76–85.

Enfors, S., Jahic, M., Rozkov, A., Xu, B., Hecker, M., & Ju, B. (2001). Physiological responses to mixing in large scale bioreactors. *Journal of Biotechnology*, *85*, 175–185.

Gaddis, E. S., & Vogelpohl, A. (1986). Bubble formation in quiescent liquids under constant flow conditions. *Chemical Engineering Science*, *41*(1), 97–105.

Garcia-Ochoa, F., & Gomez, E. (2009). Bioreactor scale-up and oxygen transfer rate in microbial processes: An overview. *Biotechnology Advances*, *27*, 153–176.

Hagesaether, L., Jakobsen, H. A., & Svendsen, H. F. (2002). A model for turbulent binary breakup of dispersed fluid particles. *Chemical Engineering Science*, *57*(16), 3251–3267.

Haringa, C., Deshmukh, A. T., Mudde, R. F., & Noorman, H. J. (2017). Euler-Lagrange analysis towards representative down-scaling of a 22 m^3 aerobic *S. cerevisiae* fermentation. *Chemical Engineering Science*, *16*, 652–663.

Haringa, C., Tang, W., Deshmukh, A. T., Xia, J., Reuss, M., Heijnen, J. J., … Noorman, H. J. (2016). Euler-Lagrange computational fluid dynamics for (bio)reactor scale-down: An analysis of organism life-lines. *Engineering in Life Sciences*, *16*, 1–29.

Hewitt, C. J., & Nienow, A. W. (2007). The scale-up of microbial batch and fed-batch fermentation processes. *Advances in Applied Microbiology*, *62*, 105–135.

Ishii, M., & Zuber, N. (1979). Drag coefficient and relative velocity in bubbly, droplet or particulate flows. *AIChE Journal*, *25*(5), 843–855.

Junker, B. H. (2004). Scale-up methodologies for *Escherichia coli* and yeast fermentation processes. *Journal of Bioscience and Bioengineering*, *97*(6), 347–364.

Junne, S., Klingner, A., Itzeck, D., Brand, E., & Neubauer, P. (2012). *Consistency of Scale-Up from Bioprocess Development to Production. In* Biopharmaceutical Production Technology (pp. 511–543). Weinheim, Germany: Wiley-VCH Verlag GmbH & Co. KGaA.

Käß, F., Junne, S., Neubauer, P., Wiechert, W., & Oldiges, M. (2014). Process inhomogeneity leads to rapid side product turnover in cultivation of *Corynebacterium glutamicum*. *Microbial Cell Factories*, *13*(1), 6.

Kálal, Z., Jahoda, M., & Fort, I. (2014). Modelling of the bubble size distribution in an aerated stirred tank: Theoretical and numerical comparison of different breakup models. *Chemical and Process Engineering*, *35*(3), 331–348.

Kita, K., Konishi, K., & Anraku, Y. (1984). Terminal oxidases of *Escherichia coli* aerobic respiratory chain. *Journal of Biological Chemistry*, *259*(5), 3368–3374.

Kumar, S., & Ramkrishna, D. (1996). On the solution of PBE by discretization-I. A fixed pivot technique. *Chemical Engineering Science*, *51*(8), 1311–1332.

Kuschel, M., Siebler, F., & Takors, R. (2017). Lagrangian trajectories to predict the formation of population heterogeneity in large-scale bioreactors. *Bioengineering*, *4*(2), 27.

Kusumoto, K., Sakiyama, M., Sakamoto, J., Noguchi, S., & Sone, N. (2000). Menaquinol oxidase activity and primary structure of cytochrome bd from the amino-acid fermenting bacterium *Corynebacterium glutamicum*. *Archives of Microbiology*, *173*(5–6), 390–397.

Kysela, B., Konfrst, J., Chara, Z., Sulc, R., & Jasikova, D. (2017). Evaluation of the turbulent kinetic dissipation rate in an agitated vessel. *European Physical Journal Conferences*, *02062*, 1–4.

Laakkonen, M., Alopaeus, V., & Aittamaa, J. (2006). Validation of bubble breakage, coalescence and mass transfer models for gas-liquid dispersion in agitated vessel. *Chemical Engineering Science*, *61*(1), 218–228.

Laakkonen, M., Moilanen, P., Alopaeus, V., & Aittamaa, J. (2007a). Modelling local bubble size distributions in agitated vessels. *Chemical Engineering Science*, *62*(3), 721–740.

Laakkonen, M., Moilanen, P., Alopaeus, V., & Aittamaa, J. (2007b). Modelling local gas–liquid mass transfer in agitated vessels. *Chemical Engineering Research and Design*, *85*(5), 665–675.

Lapin, A., Schmid, J., & Reuss, M. (2006). Modeling the dynamics of *E. coli* populations in the three-dimensional turbulent field of a stirred-tank bioreactor—a structured–segregated approach. *Chemical Engineering Science*, *61*, 4783–4797.

Leuchtenberger, W., Huthmacher, K., & Drauz, K. (2005). Biotechnological production of amino acids and derivatives: Current status and prospects. *Applied Microbiology and Biotechnology*, *69*(1), 1–8.

Lindner, S. N., Seibold, G. M., Henrich, A., Krämer, R., & Wendisch, V. F. (2011). Phosphotransferase system-independent glucose utilization in *Corynebacterium glutamicum* by inositol permeases and glucokinases. *Applied and Environmental Microbiology*, *77*(11), 3571–3581.

Löffler, M., Simen, J. D., Jäger, G., Schäferhoff, K., Freund, A., & Takors, R. (2016). Engineering *E. coli* for large-scale production—strategies considering ATP expenses and transcriptional responses. *Metabolic Engineering*, *38*, 73–85.

Luo, H., & Svendsen, H. F. (1996). Theoretical model for drop and bubble breakup in turbulent dispersions. *AIChE Journal*, *42*(5), 1225–1233.

Montante, G., Moštěk, M., Jahoda, M., & Magelli, F. (2005). CFD simulations and experimental validation of homogenisation curves and mixing time in stirred Newtonian and pseudoplastic liquids. *Chemical Engineering Science*, *60*(8-9), 2427–2437.

Morchain, J., Gabelle, J. C., & Cockx, A. (2014). A coupled population balance model and CFD approach for the simulation of mixing issues in lab-scale and industrial bioreactors. *American Institute of Chemical Engineers*, *60*, 27–40.

Morrison, C., & Lähteenmäki, R. (2017). Public biotech in 2016—the numbers. *Nature Biotechnology*, *35*(7), 623–629.

Neubauer, P., Cruz, N., Glauche, F., Junne, S., Knepper, A., & Raven, M. (2013). Consistent development of bioprocesses from microliter cultures to the industrial scale. *Engineering in Life Sciences*, *13*, 224–238.

Nieß, A., Löffler, M., Simen, J. D., & Takors, R. (2017). Repetitive short-term stimuli imposed in poor mixing zones induce long-term adaptation of *E. coli* cultures in large-scale bioreactors: Experimental evidence and mathematical model. *Frontiers in Microbiology*, *8*(June), 1–9.

Pigou, M., & Morchain, J. (2015). Investigating the interactions between physical and biological heterogeneities in bioreactors using compartment, population balance and metabolic models. *Chemical Engineering Science*, *126*, 267–282.

Roels , & J. A. (1983). *Energetics and Kinetics in Biotechnology*. Amsterdam: Elsevier Biomedical Press.

Rosseburg, A., Fitschen, J., Wutz, J., Wucherpfennig, T., & Schlüter, M. (2018). Hydrodynamic inhomogeneities in large scale stirred tanks – influence on mixing time. *Chemical Engineering Science*, *188*, 208–220.

Rushton, J. H., Costich, E. W., & Everett, H. J. (1950). Power characteristics of mixing impeller. *Chemical Engineering Progress*, *46*, 395–404.

Scargiali, F., D'Orazio, A., Grisafi, F., & Brucato, A. (2007). Modelling and simulation of gas–liquid hydrodynamics in mechanically stirred tanks. *Chemical Engineering Research and Design*, *85*(5 A), 637–646.

Schmidt, F. R. (2005). Optimization and scale up of industrial fermentation processes. *Applied Microbiology and Biotechnology*, *68*, 425–435.

Takors, R., Bathe, B., Rieping, M., Hans, S., Kelle, R., & Huthmacher, K. (2007). Systems biology for industrial strains and fermentation processes—Example: Amino acids. *Journal of Biotechnology*, *129*(2), 181–190.

Tomiyama, A., Kataoka, I., Zun, I., & Sakaguchi, T. (1998). Drag coefficients of single bubbles under normal and micro gravity conditions. *JSME International Journal Series B*, *41*(2), 472–479.

Vasconcelos, J. M. T., Alves, S. S., & Barata, J. M. (1995). Mixing in gas-liquid contactors agitated by multiple turbines. *Chemical Engineering Science*, *50*(14), 2343–2354.

Vrábel, P., Van Der Lans, R. G. J. M., Van Der Schot, F. N., Ch, K., Luyben, A. M., Xu, B., & Enfors, S. (2001). CMA: Integration of fluid dynamics and microbial kinetics in modelling of large-scale fermentations. *Chemical Engineering Journal*, *84*, 463–474.

Wiedmann, J. A. (1983). Zum überflutungsverhalten zwei- und dreiphasig betriebener Rührreaktoren. *Chemie Ingenieur Technik*, *55*(9), 689–700.

Xueming, S., Xiaoling, L., & Yulin, L. (2008). Experimental study of influence of the impeller spacing on flow behaviour of double-impeller stirred tank. *The Canadian Journal of Chemical Engineering*, *81*(6), 1239–1245.

SUPPORTING INFORMATION

Additional supporting information may be found online in the Supporting Information section.

How to cite this article: Kuschel M, Takors R. Simulated oxygen and glucose gradients as a prerequisite for predicting industrial scale performance a priori. *Biotechnology and Bioengineering*. 2020;117:2760–2770. https://doi.org/10.1002/bit.27457